

Crystal defects in SiC wafers and a new X-ray topography system

Kazuhiko Omote*

1. Introduction

High-voltage and high-efficiency power devices are in strong demand as a way of decreasing energy consumption in a wide range of industrial and consumer products. Wide band gap semiconductors such as SiC, GaN, and diamond are candidates for producing these next generation power devices. Table 1 indicates the basic physical properties for these materials compared to Si. These materials have a much higher breakdown voltage and are expected to be used in future equipment requiring compact and low-loss conversion devices. Among these materials, SiC is the most promising candidate and is expected to be used in a wide range of power device applications in the near future.

The band gap of SiC is approximately three times greater than Si and has a breakdown electric field strength nearly 10 times higher than Si as shown in Table 1. These characteristics result from the extremely strong atomic bonds in the crystal. Due to the strong atomic bonds, SiC will not melt at its original composition, even at high temperatures. Even at a temperature of more than 2,800°C, at 100 atm, SiC remains in a phase in which a Si melt containing approximately 19% C coexists with solid graphite. Unlike Si, a direct crystal growth method from the melt is not possible with SiC. This poses significant difficulties in growing the large-diameter single crystals required for device production. For these reasons, single crystals are now mainly grown by the sublimation method (modified Lely method)⁽¹⁾. SiC sublimates at approximately 2,500°C and grows on a single crystal seed placed in an environment of approximately 2,200°C. The sublimation rate determines crystal growth rate. Since this process involves extremely high temperatures, it entails various problems, including impurities migrated into the substrate crystal and crystal

defects caused by thermal stress. In addition, SiC has many polytypes with different atomic layer stacking. It is important to control proper crystal polytype growth and avoid twinning. Recent improvements in crystal growth methods have solved many of these problems. In particular, the occurrences of micropipes, crystal defects that can fatally damage device performance, have been reduced to near zero. Current methods are capable of producing 6-inch large-diameter wafers. However, crystal growth process at such high temperatures is difficult and expensive. In addition, growth crystals still contain numerous defects, including dislocations. Further technological advances are required, including investigations of other methods such as solution growth and gas phase growth.

Since the crystal growth is a high temperature process, it is difficult to control the impurity concentrations during bulk single crystal growth, which is essential for semiconductor device fabrication. The most important progress was achieved by introducing a step-flow epitaxy⁽²⁾, which is homoepitaxial growth using the CVD method. The step-flow mechanism that induces crystal growth along the steps on the atomic surface using a hexagonal SiC crystal wafer 4° to 8° off-cut relative to the c plane. This method can produce epitaxial layers with satisfactory crystallinity even at 1,500°C, which is much lower than the growth temperature of the single crystal. This method also allows precise control of both p and n conductivity that are the key for the device performance. It is now possible to acquire commercial SiC devices according to these improvements.

2. SiC crystal structure and crystal defects

As mentioned, SiC has many polytypes. Of these, typical crystal forms with high potential for device

Table 1. Basic physical properties for device performances of 4H-SiC, Si, GaN, and diamond.

	Si	4H-SiC	GaN	Diamond
Band gap (eV)	1.12	3.26	3.42	5.47
Electron mobility (cm ² /Vs)	1350	1000	1500	2000
Breakdown voltage (MV/cm)	0.3	2.8	3	8
Saturated drift velocity (cm/s)	1.0×10 ⁷	2.2×10 ⁷	2.4×10 ⁷	2.5×10 ⁷
Thermal conductivity (W/cmK)	1.5	4.9	1.3	20

* X-ray Research Laboratory, Rigaku Corporation.

applications include cubic 3C-SiC and hexagonal 4H-SiC and 6H-SiC. These three polytypes have different stacking sequences along the *c* axis. The stacking sequences of the Si and C atoms of these structures have the repeating patterns of ABCA, ABCBA, and ABCACBA, respectively, as shown in Fig. 1. Since SiC has many polymorphs differing only in stacking sequence, it readily forms defects known as stacking faults, caused by mixing different stacking patterns during crystal growth. Since the step-flow epitaxy⁽²⁾ mentioned above is associated with growth in the directions of the *a* and *b* axes as well as in the direction of the *c* axis, a consistent stacking sequence can be observed, allowing growth of an epitaxial film containing few stacking faults. Figure 2 shows the crystal orientation and *c*-axis off-angle relative to the orientation flat for the 4H-SiC wafer, currently the most recent development to enter actual device applications. These specifications are defined in the SEMI standard⁽³⁾. Commercially-available wafers are generally manufactured in accordance with this standard.

As discussed in the previous section, SiC crystals are grown under conditions at extremely high temperatures. The wafers currently produced contain numerous crystal defects. Table 2 summarizes the types of dislocations in hexagonal SiC crystals. The Burgers vector of the

threading screw dislocation is the same as the *c*-axis of the crystal. Depending on crystal growth conditions, dislocations may be formed with a large Burgers vector, corresponding to its integer multiples. These defects are called micropipes⁽⁴⁾ and are characterized by minute holes measuring over 10 μm in diameter at the dislocation center. These dislocations fatally influence device characteristics. However, recent advances in growth control techniques have made it possible to produce 4-inch wafers containing virtually no micropipes.

In addition, the active region of SiC devices is not formed directly on the wafer obtained from bulk growth; rather, it is formed on the film by step-controlled epitaxy on the substrate. Most threading screw and edge dislocations in the substrate are known to be carried into the epitaxial film, while 95% or more of basal plane dislocations are converted to threading edge dislocations⁽⁵⁾. Certain threading screw dislocations also initiate stacking faults and large defects referred to as carrot defects⁽⁶⁾.

Since numerous crystal defects including dislocations are inevitable with SiC wafers made by current technologies, fabrication of devices must assume that crystals have such defects. Thus, a key issue is to clarify the relationship between crystal defects and device characteristics. This also helps to optimize the yield and life of manufactured devices. However, ordinary crystal defect inspections like those based on etching are destructive and cannot provide a one-to-one

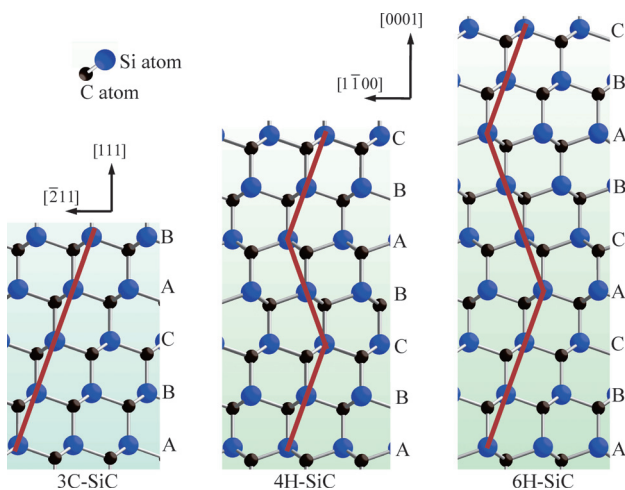


Fig. 1. Crystal structures of 3C-, 4H-, and 6H-SiC. Each has a different stacking sequence perpendicular to the close packed plane.

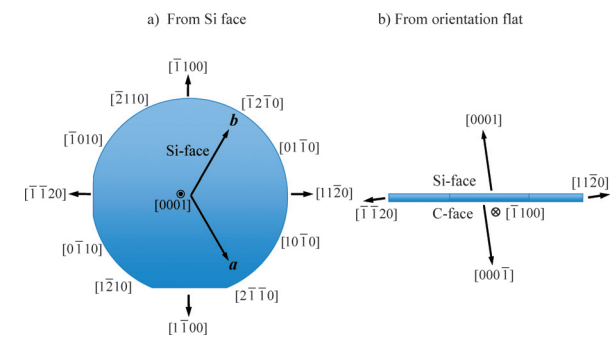


Fig. 2. Relationship between the orientation flat and crystallographic orientation of 4H-SiC wafer as defined in the SEMI standard. (a) Viewed from Si plane; (b) viewed from first orientation flat

Table 2. Types of dislocations formed in hexagonal SiC and typical dislocation density in commercially available wafers.

	Dislocation direction	Slip plane	Burgers vector	Dislocation density (cm ⁻²)
Threading screw dislocation	$\langle 0001 \rangle$	–	$\langle 0001 \rangle$ or doubled	10 ² –10 ³
Threading edge dislocation	$\langle 0001 \rangle$	(1100)	1/3 $\langle 1120 \rangle$	Order of 10 ³ to 10 ⁴
Basal plane dislocation	Arbitrary in (0001) plane, stable orientation: $\langle 1120 \rangle$	(0001)	1/3 $\langle 1120 \rangle$	Order of 10 ³ to 10 ⁴

correspondence between the presence of defects and device characteristics. X-ray measurements, on the other hand, are capable of evaluating the substrates and epitaxial films nondestructively. In particular, measuring the positions and types of defects on the wafer with X-ray topography makes it possible to compare and investigate device characteristics and crystal defects at the same position. In addition, since X-ray topography can also measure product wafers themselves, it is expected to serve as an effective quality control tool for wafers and epitaxial films.

3. SiC crystal defect measurement by X-ray topography

Figure 3 shows typical measurement geometries for X-ray topography. The transmission topography shown in (a) is called the Lang method⁽⁷⁾ and is most widely used for measuring crystal defects such as dislocations and stacking faults. As shown in Fig. 4, incident X-rays are transmitted and diffracted by a certain lattice plane

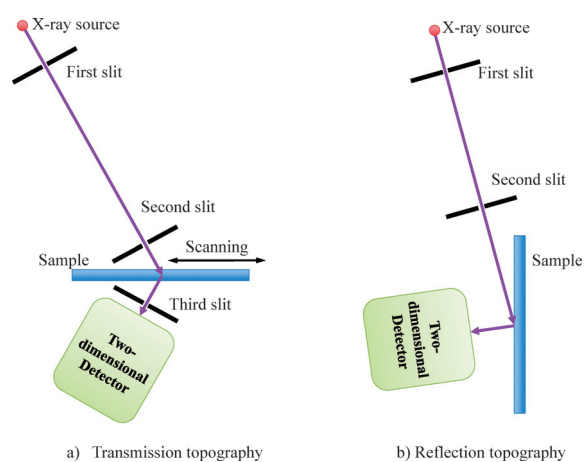


Fig. 3. Schematic diagram of X-ray topography.
(a) Transmission geometry; (b) reflection geometry

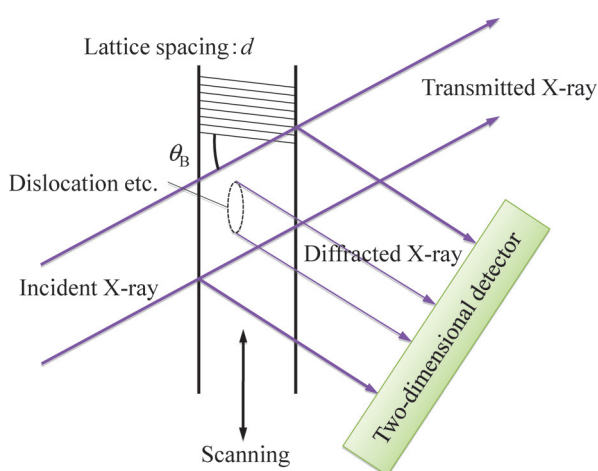


Fig. 4. Schematic diagram of Lang topography.
Scanning the sample in the vertical direction in the figure allows imaging of internal crystal defects over a wide area of the sample.

at the angle satisfying the Bragg condition, and the diffracted X-rays are imaged on the two-dimensional detector. The original Lang method used X-ray film as a two-dimensional detector and scanned the sample and the film simultaneously to record an X-ray diffraction image of a large area (entire crystal). Here, any defects found in the crystal are detected as faults in the X-ray diffraction image. Figure 5 illustrates this mechanism in detail. A perfect crystal without defects diffracts parallel X-ray components only several arcsec to 10 arcsec at a probability of nearly 1, whereas other divergent components pass through the sample without diffraction. On the other hand, incident X-ray components with an angular divergence of 100 arcsec or larger can be diffracted around dislocations, because the crystal lattice plane can be deformed caused by the stress from the dislocation. Since typical measurements based on the Lang method use moderately divergent X-rays dislocations are able to contribute to the overall diffraction. Therefore, the diffraction intensity in the area containing dislocations is observed to be stronger. In contrast, use of a crystal collimator or very low divergence incident X-rays of several arcsec (close to the diffraction width of the crystal), as is the case with a synchrotron source, the Bragg condition is not satisfied near the dislocations, and the observed diffraction intensity becomes weaker. In either case, if the distance between dislocations is ten to several tens of micrometers, each dislocation is clearly resolved in the topographic image.

Figure 6 shows a transmission topography image with the 1100 reflection, obtained by scanning the entire 3-inch SiC wafer using the Mo $K\alpha_1$ line in a laboratory (negative image with higher intensity indicated darker). Here, an X-ray film was used as the two-dimensional detector, and the sample and the X-ray film were simultaneously scanned in the geometry shown in Fig. 3(a). As shown in the enlarged view on the right, dark linear dislocations are clearly resolved. These are images of the basal plane dislocations or threading edge dislocations as classified in Table 2. The spotted parts are points formed where threading screw dislocations penetrate to the surface. These dislocations appear dark (higher diffraction intensity) because divergent components of the incident X-rays contribute to the diffraction, as described in Fig. 5.

As this example shows, defect density of recent SiC wafers has improved significantly, and each dislocation is clearly visible. However, Fig. 6 shows two areas where dislocations concentrate to form dark blotches. They result from micropipes as discussed in the previous section. The paired horizontal dark lines are called simultaneous diffractions, occurring when reflections other than the intended 1100 simultaneously satisfy the Bragg condition. The paired dark lines are corresponding to the Mo $K\alpha_1$ and $K\alpha_2$, respectively. Such a simultaneous diffraction constitutes the background and is undesirable. However, with Lang method, in which a large area is measured with large photographic

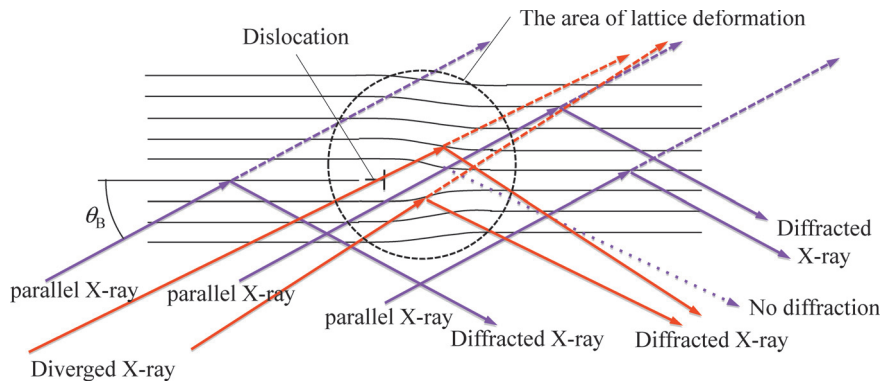


Fig. 5. Effects on X-ray diffraction when dislocations in the crystal generate deformation in the crystal lattice.

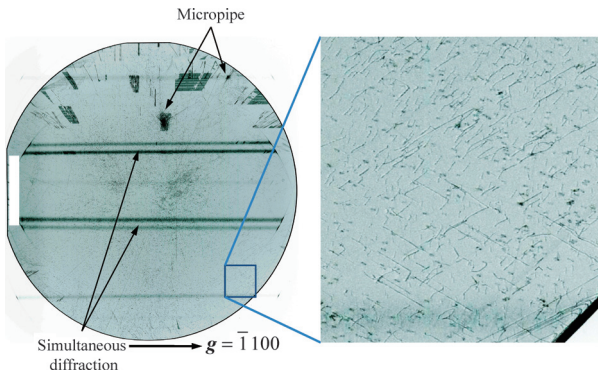


Fig. 6. Transmission topography images of 3-inch 4H-SiC wafer measured with the 1100 reflection by Lang method. Each dislocation is clearly resolved. Measured by a conventional X-ray sealed tube and a photographic film. The measurement time was 10 hours or longer.

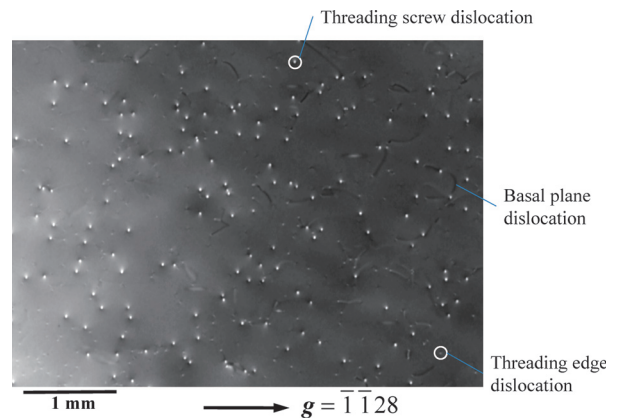


Fig. 7. Topography image of SiC wafer measured in reflection geometry with the 1128 reflection using synchrotron source (PF BL-15C) using a nuclear plate. Basal plane dislocations, threading screw dislocations, and threading edge dislocations can be recognized.

film, this is inevitable. This measurement uses a 50-kV, 40-mA, sealed tube as the X-ray source and requires 10 hours for the exposure. Conventional methods based on photographic film require the use of long exposure times.

As discussed earlier, the active region of a SiC device is formed in the epitaxial layer fabricated on the substrate. Therefore, it is even more critical to evaluate the crystal defects in the epitaxial layer using reflection topography as illustrated in Fig. 3(b). Figure 7 shows the results of reflection topography for an epitaxial film on a 3-inch wafer measured at the BL-15C beamline at the Photon Factory. This measurement uses a Si 111 monochromator to extract X-rays with a wavelength of 1.5 Å. The X-ray image was detected on a nuclear plate allowing measurements of extremely high resolution (1 μm or less). Since the substrate measured has an off-angle of 4°, the X-ray incident angle for the 1128 reflection is approximately 9°. This angle determines the penetration (analysis) depth, which is approximately 10 μm in this example. As shown in Fig. 7 we can recognize three types of dislocations in the SiC crystal. First, the large, bright spots correspond to threading screw dislocations. Since they are associated with large strain in the surrounding areas, strongly contrasted areas

are visible for this dislocation. Basal plane dislocations appear as bright or dark lines. The small, barely visible spots with weak contrast correspond to threading edge dislocations. Since measurements with synchrotron source use a parallel X-ray beam, diffraction intensity from areas with lattice distortion near dislocations is weak and is observed as bright areas.

So far, we have discussed detection of SiC dislocations from transmission and reflection topographies. It enables non-destructive quantitative measurements of dislocations and provides a useful way to examine the relationship between crystal defects and device characteristics.

4. New X-ray topography system

X-ray topography, which has been in use for over half a century⁽⁷⁾, was significantly improved upon the advent of synchrotron sources, which also benefited other X-ray diffraction systems. On the other hand, recent progress in technologies for X-ray sources, optics, and two-dimensional detectors, have also contributed to significant improvements in performance of laboratory equipment. In order to measure a topography image with a characteristic $K\alpha_1$ line in the laboratory, we

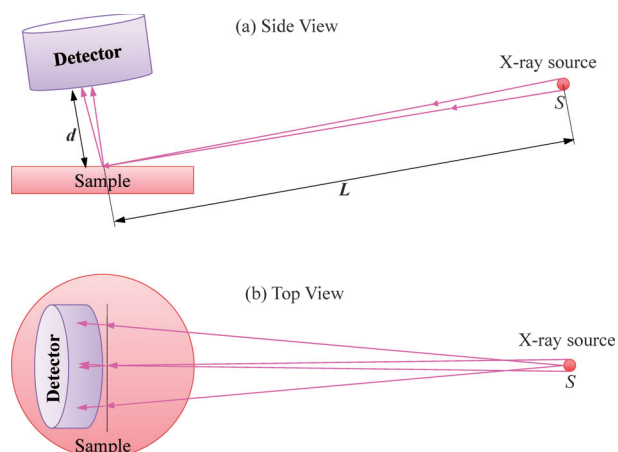


Fig. 8. Geometrical relations determining topography spatial resolution: (a) Side view; spatial resolution is determined by diffraction width of the crystal δ and distance d between the sample and detector. (b) Top view; relationship among size S of the X-ray source, distance L between the X-ray source and the sample, and d restricts the spatial resolution.

must place a collimator on the incident side to prevent diffraction by the characteristic $K\alpha_2$ line. It is crucial to avoid overlapping diffraction images from $K\alpha_1$ and $K\alpha_2$. Conventionally, this is achieved by inserting a slit as shown in Fig. 3. Recently, multilayer X-ray mirrors with parabolic surfaces have been developed. Monochromatic X-rays are obtained by Bragg reflection of the multilayer and they are also converted to a collimating beam by the reflection on a parabolic surface. This technology is widely used in the field of X-ray diffraction⁽⁸⁾. The new optic makes it possible to obtain diffraction images of a single crystal sample using only the $K\alpha_1$ line, without mechanical slits. A microfocus X-ray source with high brilliance⁽⁹⁾ is required to take advantage of the performance of the optics. Consequently, Rigaku has developed high-brilliance rotating anode X-ray sources such as the MicroMax-007HF and the FR-X to take full advantage of these optics.

High-brilliance, microfocus X-ray sources are significant for topography as well. Apart from the spatial resolution of the detector, topography resolution is determined mainly by the size of the X-ray source and the divergence of the beam, as shown in Fig. 8. In the plane containing the incident and diffracted X-rays (side view), the beam spread on the detector is expressed as $\delta \cdot d$, where the angular divergence of the X-rays denotes δ and the distance between the sample and the detector d . Since the diffraction width of a crystal is usually several arcsec, we can easily achieve $\delta \cdot d \leq 1 \mu\text{m}$. On the other hand, in the plane perpendicular to the previous plane (top view), the spread on the detector is determined entirely by geometrical arrangement. The spread at the detector is given by $d/L \times S$, where S is the X-ray source size and L the distance from source to sample position. Since the diameter of the MicroMax-007HF focal spot is $70 \mu\text{m}$ in diameter, by assuming $L=800 \text{ mm}$ and $d=10 \text{ mm}$, we obtain $d/L \times S < 1 \mu\text{m}$.



Fig. 9. Conventional topography system for 300-mm wafers.

This means measurements with a resolution of $1 \mu\text{m}$ are possible while the detector has enough special resolution.

Imaging techniques, such as topography, require not only collimated and monochromatic X-rays, but also homogeneity (uniformity) of the beam. In other words, inhomogeneities in the X-ray beam from the multilayer mirror will overlap with the diffraction (defect) image of the sample. Recent developments in precise figure control make it possible to produce an extremely uniform X-ray beam. The error from the design value of the surface figure (figure error) can now be kept at 4 arcsec (2 arcsec in the best case) or less. This angular error is smaller than the diffraction width of a typical single crystal and has little effect on the topography image, as shown by data presented later in this paper.

For X-ray two-dimensional detectors, we also have seen progress with charge coupled (CCD) and pixel-array detectors. Spatial resolution is a particularly important characteristic for X-ray topography. Conventional X-ray films provide a resolution of several micrometers, while nuclear plates provide a resolution of $1 \mu\text{m}$. It is not easy to produce such a high-resolution detector, however, as we will show later, a CCD detector developed by Rigaku is capable of resolving each dislocation in a topography image. This new digital detector provides the major advantage of online data acquisition. Further improvements for resolution and detection sensitivity are expected.

Figure 9 shows a topography system (XRT-300) capable of measuring up to 300 mm wafers based on the original Lang method. An imaging plate (IP) or X-ray film is used as the detector. To cover the entire height of the 300-mm wafer in the measurement view, the distance from the X-ray source to the sample is elongated to 1.4 m. Here, the sample is held between two films and manually attached to the sample cassette in the vertical position. It is difficult to create an automatic sample transfer system with this configuration. The data is read from the IP or X-ray film and it is also difficult to access the data online. In order to overcome these problems, Rigaku has developed a new X-ray

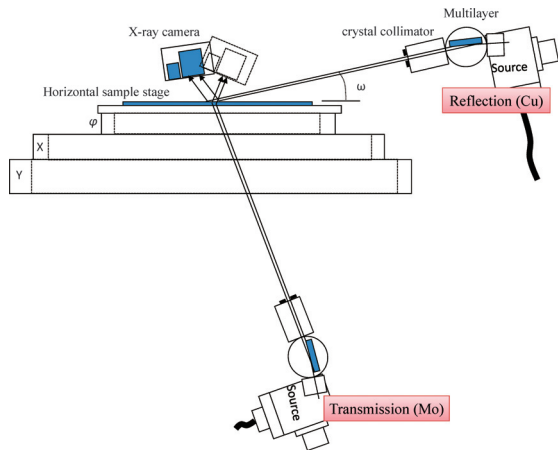


Fig. 10. Schematic diagram of the new X-ray topography system. The X-ray sources and optics move to locations suitable for transmission and reflection geometries.

topography system using the current progress of the technologies discussed earlier. Figure 10 is a schematic diagram of the new system. The sample is held horizontally, and the X-ray source and the multilayer film are rotated together to satisfy Bragg conditions for the reflection plane, which we would like to measure. Since the multilayer film produces a monochromatic, parallel X-ray beam, this new system does not require a slit near the sample. The sample is held horizontally and it is easy to support using an automatic sample transfer system. In addition, there is a computer-controlled mechanism to exchange between Mo source and a Cu source (MicroMax-007HF (DW), 1.2kW). The user can easily switch between transmission topography to observe the defects in the entire crystal and reflection topography to observe defects near the surface.

Figures 11 and 12 show the internal structure and external appearance of the system developed based on the concept described here. Figure 11 shows the state of the goniometer in reflection topography. In transmission topography, θ_s is directed downward (to the negative side) at which X-rays are coming from lower side of the sample to generate a diffraction image for measurement by the two-dimensional detector. For the two-dimensional detector, two cameras can be simultaneously mounted: a high-sensitivity camera with a pixel size of $5.4\mu\text{m}$ and a high-resolution camera with a pixel size of $2.16\mu\text{m}$. The sample stage holds samples with a maximum size of 300 mm and is compatible with the automatic sample transfer system. It can be replaced with a stage with a Z-axis (perpendicular to the sample surface) dedicated to reflection topography or a 450-mm diameter Si wafer stage.

Figure 13 shows a $\text{MoK}\alpha_1$ transmission topography image of a SiC wafer measured with this system. As with the photographic film image shown in Fig. 6, each dislocation is clearly resolved. The measurement was made with a high-sensitivity camera with a pixel size

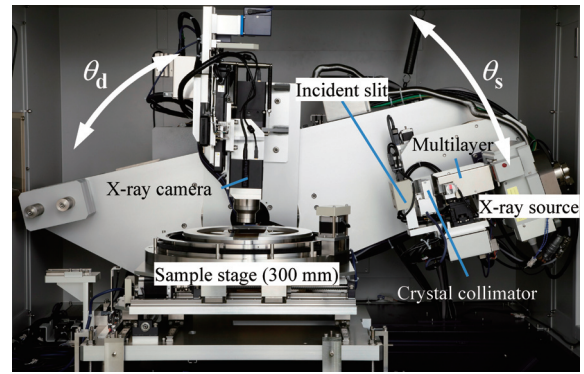


Fig. 11. Internal structure of the new X-ray topography system including the goniometer and the sample stage.



Fig. 12. External appearance of the new X-ray topography system.

of $5.4\mu\text{m}$. Since, the detection area of this detector does not cover the entire wafer, the sample was measured by the TDI (Time-delay integration) technique, in which the sample is scanned as shown in Fig. 3 (a) and the charged packets are moved synchronously with sample movement while the CCD itself is fixed. The area that can be measured in a single scan is shaped like a ribbon of the width corresponding to the height of the X-ray camera window (approximately 18mm in height). For measuring a larger area, multiple scans are required, with the sample moved by the height of the camera window for each scan. The scan speed in the measurement shown in Fig. 13 is 2mm/sec. It requires approximately 4minutes to measure the entire 3-inch wafer. This is approximately 100 times faster than conventional systems with a 2-kW sealed X-ray tube and 10 times faster or better than one with an 18-kW rotating anode X-ray source. However, for large wafers, the required number of scans increases, and ratios with a 300-mm wafer decrease to approximately 1/3. Still, it is worth noting that the new system allows much faster measurements than conventional laboratory topography.

Figure 12 shows the results of in the reflection topography with $\text{CuK}\alpha_1$ line for the 1128 reflection of

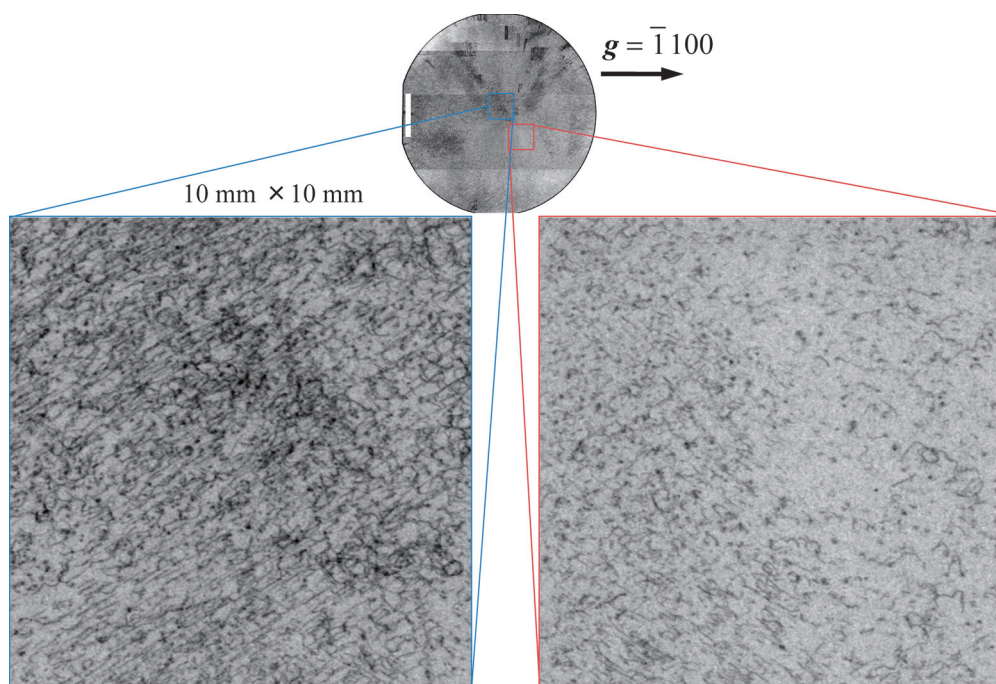


Fig. 13. Transmission topography image for 4H-SiC $\bar{1}100$ reflection measured by a high-sensitivity X-ray camera. The dislocations are imaged with sufficient contrast at scan speeds of 2 mm/sec.

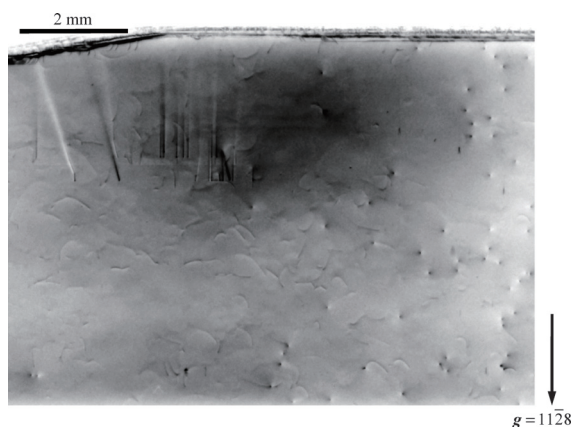


Fig. 14. Parallel beam topography with 4H-SiC 1128 reflection, using crystal collimator of Si 440 channel cut crystal. The dislocations are imaged with high contrast.

a wafer on which an epitaxial layer is grown. In order to increase sensitivity for deformation of lattice plane, we have inserted a double crystal collimator using the Si 440 reflection on the incident side and performed measurements in the (+, -) configuration. The Bragg angle for the Si 440 reflection with $\text{CuK}\alpha_1$ is 53.36° , while the Bragg angle for the 4H-SiC 1128 reflection is 52.36° . These two values are extremely close, and high-resolution measurement is possible with small wavelength dispersion (pseudoparallel geometry). In particular, this measurement used a diffraction condition slightly shifted from the Bragg peak angle of the crystal. This way we can enhance the difference in diffraction intensity around dislocations. As a result, the linearly extending basal plane dislocations and spotted threading

screw dislocations associated with dark and bright contrast can be recognized in the topography image. In the present measurement, the angle of the incident X-rays was approximately 17° and penetration depth of the X-ray is about $20\mu\text{m}$, whereas the thickness of the epitaxial film of the sample was approximately $10\mu\text{m}$. Thus, it is not clear that the basal plane dislocations exist in the substrate or epitaxial film. Here, when we measured the 0004 locking curve of this wafer, the full width at half maximum (FWHM) was approximately 10 arcsec, which is very close to the theoretical value for the perfect SiC crystal. The imaging of so many dislocations (Fig. 12) despite the small FWHM demonstrates that rocking curve measurements are not sufficient to evaluate wafers at this quality and that dislocation measurements by topography should be effective.

5. Summary

This article discusses various types of crystal structures and crystal defects and examples of related topography observations for SiC wafers—a substrate which is expected to play a major role in next-generation power devices. It also describes a new topography system, which incorporates recently developed key components, such as microfocus rotating anode X-ray sources, multi-layer optics, and electronic detectors. This new system should be useful not only for research and development, but also for wafer inspection and/or quality control. The same should hold true for GaN and AlN crystals that have also attracted attention as new device materials but whose high-quality single crystals have been difficult to grow. Although GaN is in use for practical applications (e.g., LED lighting) with

crystals grown on sapphire substrates, the demand for high-quality bulk single crystal substrates is increasing in applications for power devices. Because the liquid phase of GaN with a consistent composition requires temperatures of 1,500°C and pressures of 10,000 atm, it is not as easy to obtain as with SiC. Therefore, lots of studies have been made to grow GaN bulk single crystals by various methods, gas phase growth, solution growth, etc⁽¹⁰⁾⁻⁽¹²⁾. The problems posed for crystal quality are the same as for SiC, and the need for X-ray topography crystal evaluations is expected to develop for GaN devices as well.

References

- (1) Yu. M. Tairov and V. F. Tsvetkov: *J. Cryst. Growth*, **43** (1978), 209–212.
- (2) H. Matsunami and T. Kimoto: *Mater. Sci. Eng.*, **R20** (1997), 125–166.
- (3) SEMI (Semiconductor Equipment and Materials International) International Standards M55–0308.
- (4) N. Otani, J. Takahashi, M. Katsuno, H. Hoshino and M. Kanaya: *Mater. Res. Sic. Symp. Proc.*, **510** (1998), 37–45.
- (5) H. Hara, Y. Sano, H. Mimura, K. Arima, A. Kubota, K. Yagi, J. Murata and K. Yamauchi: *J. Electron. Mater.*, **35** (2006), L11–L14.
- (6) H. Tsuchida, M. Ito, I. Kamata and M. Nagano: *Phys. Status Solidi*, **B246** (2009), 1553–1568.
- (7) A. R. Lang: *Acta Cryst.*, **12**(1959), 249–250.
- (8) M. Shuster and H. Gobel: *Adv. X-ray Anal.*, **39** (1997), 57–71.
- (9) K. Shimizu, K. Omote: *Rigaku Journal (English version)*, **24** (2008), No. 1, 1–9.
- (10) R. Dwilinski, R. Doradzinski, J. Garczynski, L. P. Sierzputwski, A. Puchalski, Y. Kanbara, K. Yagi, H. Minakuchi and H. Hayashi: *J. Cryst. Growth*, **310** (2008), 3911–3916.
- (11) R. P. Vaudo, X. Xu, C. Loria, A. D. Salant, J. S. Flynn and G. R. Brandes: *Phys. Stat. Sol.*, **A194** (2002), 494–497.
- (12) F. Kawamura, M. Morishita, M. Tampo, M. Imade, M. Yoshimura, Y. Kitaoka, Y. Mori and T. Sasaki: *J. Cryst. Growth*, **310** (2008), 3946–3949.